A Soft-Switched DC/DC Converter for Fuel Cell Vehicle Applications*

Gui-Jia Su, Donald J. Adams
Oak Ridge National Laboratory

Fang Z. Peng
Michigan State University

Hui Li
Tyco Electronics

ABSTRACT

Fuel cell–powered electric vehicles (FCPEV) require an energy storage device to start up the fuel cells and to store the energy captured during regenerative braking. Low-voltage (12 V) batteries are preferred as the storage device to maintain compatibility with the majority of today's automobile loads. A dc/dc converter is therefore needed to interface the low-voltage batteries with the fuel cell–powered higher-voltage dc bus system (255 V ~ 425 V), transferring energy in either direction as required. This paper presents a soft-switched, isolated bi-directional dc/dc converter developed at Oak Ridge National Laboratory for FCPEV applications. The converter employs dual half-bridges interconnected with an isolation transformer to minimize the number of switching devices and their associated gate drive requirements. Snubber capacitors including the parasitic capacitance of the switching devices and the transformer leakage inductance are utilized to achieve zero-voltage switching (ZVS). Therefore, no extra resonant components are required for ZVS, further reducing component count. The inherent soft-switching capability and the low component count of the converter allows high power density, efficient power conversion, and compact packaging. A prototype rated at 1.6 kW was built and successfully tested. Experimental results confirmed soft-switching operation and an average model based analysis.

INTRODUCTION

The automotive industry is at the dawn of a new era in alternative propulsion. Fuel cells show great promise as the primary power source for next-generation propulsion, because they generate clean electricity directly and efficiently while leaving only nonpolluting byproducts—water and heat [1]. An auxiliary energy storage device is required for start-up and for storing the energy captured by regenerative braking in electric vehicle applications, because the present fuel cell technology lacks energy storage capability. One way to accomplish this is to utilize the vehicle 12 V battery with a bi-directional dc-dc converter to maintain compatibility with the majority of today's automobile loads, as shown in Fig.1. During vehicle starting, the high-voltage bus is boosted up to 288 V by the dc/dc converter drawing power from the 12 V battery. This high-voltage bus then supplies power for the fuel cell compressor motor expanding unit (CMEU) controller and brings up the fuel cell voltage, which in turn feeds back to the high-voltage bus to release the loading from the battery. In addition, the battery absorbs the energy captured by regenerative braking through the traction motor.

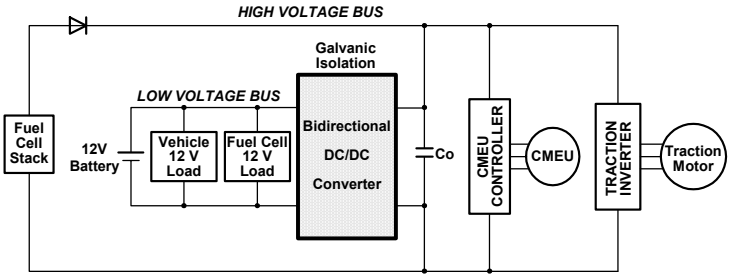

Fig.1. A conceptual diagram of a fuel cell–powered propulsion system.

This application requires a dc/dc converter with a relatively high power rating of 1.6 kW continuous, aside from bi-directional power control capability. The converter also needs to provide galvanic isolation between the low- and high-voltage buses. Further, soft switching is preferred over hard switching because of the reduced level of electromagnetic interference (EMI) and switching losses. Other expected requirements for this converter are outlined as follows.

- The terminal voltage of the battery can swing from 8

* Research sponsored by Oak Ridge National Laboratory, managed by UT-Battelle, LLC, for the U.S. Dept. of Energy under contract DE-AC05-00OR22725. The submitted manuscript has been authored by a contractor of the U.S. Government under contract DE-AC05-00OR22725. Accordingly, the U.S. Government retains a nonexclusive, royalty-free license to publish or reproduce the published form of this contribution, or allow others to do so, for U.S. Government purposes.

V to 16 V during either direction of power flow.

- The nominal voltage of the high voltage bus is 288 V, with an operating range of from 255 V to 425V.
- A maximum battery charging power of 5 kW is required for a maximum duration of 20 s during regeneration. Each such charging event is at least 1 minute apart.
- The high-voltage bus capacitance *Co* must be less than 2000 μF.
- Start-up time is less than 200 ms with load engaged when the voltage of the high-voltage bus is higher than 255 V.

Most of the existing dc/dc converter topologies are of low power or unidirectional power flow and cannot meet the requirements listed [2, 3]. Recently, some high-power, bi-directional dc/dc converters with soft-switching operation and galvanic isolation have been introduced in the literature [4–7]. These converters are regarded as candidates for automotive applications because they have the advantages of reduced switching losses and EMI. However, they are unable to achieve high power density, high reliability, and low cost because the requirements for dedicated devices and/or complicated control schemes for soft-switching result in bulky and costly implementation.

ORNL has been developing dc/dc converters that can meet the aforementioned requirements. The first generation, which was developed in 1997, employs a novel soft-switching circuit on a dual full-bridge topology [8]. While this technique could significantly improve efficiency and power density over the existing high-power dc/dc converters, the large number of active switches and associated components and complexity of control are concerns in light of the low cost and high reliability demands for automotive applications. Aiming at reducing component count and achieving soft-switching simultaneously, the second-generation dc/dc converter has been developed based on a half-bridge topology, which is the subject of this paper. The new converter employs dual half-bridges interconnected with an isolation transformer to minimize the number of switching devices and their associated gate drive requirements. Moreover, it utilizes snubber capacitors including the parasitic capacitance of the switching devices and the transformer leakage inductance to achieve zero-voltage-switching (ZVS). Therefore, no extra resonant components are required for ZVS, further reducing component count. The inherent soft-switching capability and the low component count of the converter allow high power density, efficient power conversion, and compact packaging. A 1.6 kW prototype that meets the power level, start-up time, and other requirements for FCPEVs was built and successfully tested. Experimental results confirmed both soft-switching operation and validation of an average model based-analysis. Other applications for this converter can be found in the auxiliary power supplies of other types of hybrid electric vehicles.

CONVERTER DESCRIPTION

CIRCUIT DESCRIPTION — Fig. 2 shows the bi-directional dc/dc converter, which mainly consists of dual half-bridge inverters/converters and a high-frequency transformer, *Tr*. The transformer in the high-frequency link provides the required galvanic isolation and voltage level matching. The leakage inductance of the transformer is utilized as the intermediate energy storing and transferring element. Control of the power flow between the low- and high-voltage sides can be achieved by adjusting the duty cycle, the switching frequency, and/or the phase shift angle between the transformer primary and secondary voltages, as will be discussed in detail in the following sections. When power flows from the low-voltage side (LVS) to the high-voltage side (HVS), the circuit is current-fed, or in other words, works in boost mode to keep the HVS voltage at a desired level. In the other direction of power flow, the circuit is voltage-fed, or works in buck mode, so that the battery absorbs the energy captured during the regenerative braking. The HVS switches are implemented with IGBTs, and the LVS switches are MOSFETs because of their very low on-resistance at low voltage.

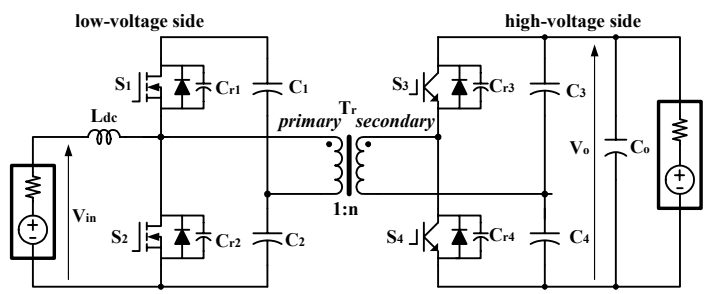

Fig. 2. The soft-switched bi-directional dual half-bridge dc-dc converter.

The leakage inductance, together with the snubber capacitors across each switch, is also utilized to provide soft switching for the switches, eliminating the problems of interaction between the leakage inductance and diode reverse recovery. The resonance between the capacitors and the inductance enables the switches to turn on under zero current and voltage, while the snubber capacitors allow them to turn off at zero voltage.

This circuit has the following features:

1. The total device rating is the same as for the dual–full-bridge alternative at the same output power.
2. Although the devices of the LVS are subject to twice the dc input voltage, this is not a serious concern because the input voltage in the anticipated application is 12 V.
3. The dual–half-bridge topology uses only half as many devices as the full-bridge topology does.

PRINCIPLES OF OPERATION — When the power flows from the LVS to the HVS, the converter works in boost/discharge mode to power the HVS load; otherwise, it works in buck mode to recharge the LVS

battery. With reference to the primary-referred equivalent circuit shown in Fig. 3, where L_s is the leakage inductance of the transformer, informative voltage and current waveforms illustrating the commutation process over a switching cycle in this mode are shown in Fig. 4. One complete switching cycle can be divided into 13 steps. Each step is described briefly as follows.

Step 1 (before t_1) — An initial state, in which S_1 and D_3 are conducting.

Step 2 (t_1 ~ t_2) — At t_1, S_1 is turned off. C_{r1}, C_{r2} and the leakage inductance of *Tr* begin to resonate, making V_{cr2} fall from V_1+V_2. V_{r1} also drops from V_1. The rate of change depends on the magnitude of I_{off}, which is the difference between I_{r1} and I_{d1} at t_1.

Step 3 (t_2 ~ t_3) — At t_2, V_{cr2} attempts to undershoot the negative rail, D_2 is therefore forward biased. During this period, S_2 can be gated on at zero current and zero voltage.

Step 4 (t_3 ~ t_4) — From t_3, I_{r1} becomes less than I_{d1}, and S_2 begins to carry the surplus current. I_{r1} keeps on decreasing until reaching zero at t_4. D_3 thereby conducts until t_4.

Step 5 (t_4 ~ t_5) — At t_4, I_{r1} changes polarity; therefore, the current passes through S_3, which was turned on when D_3 was conducting.

Step 6 (t_5 ~ t_6) — At t_5, S_3 is turned off. C_{r3} and C_{r4} begin to be charged and discharged by the transformer current, respectively. The rate of change of the voltage depends on I_{r1} at t_5.

Step 7 (t_6 ~ t_7) — At t_6, when V_{cr4} attempts to undershoot the negative rail, D_4 is forward biased. Within this period, S_4 can be gated on under zero current and zero voltage.

Step 8 (t_7 ~ t_8) — At t_7, S_2 is gated off. C_{r1}, C_{r2} and L_s begin to resonate again, making V_{cr1} discharge from V_1+V_2. V_{r1} therefore increases from $-V_2$. The rate of change now is decided primarily by the magnitude of the sum of I_{d1} and I_{r1}.

Step 9 (t_8 ~ t_9) — At t_8, when V_{cr1} attempts to undershoot the negative rail, D_1 is forward biased. I_{r1} increases until reaching zero at t_9. During this period, S_1 can be turned on at zero voltage.

Step 10 (t_9 ~ t_{10}) — At t_9, I_{r1} reverses its polarity and continues to increase until it equals I_{d1}. At the same time, the current in D_4 is commutated to S_4.

Step 11 (t_{10} ~ t_{11}) — At t_{10}, I_{r1} exceeds I_{d1}. The current is transferred from D_1 to S_1.

Step 12 (t_{11} ~ t_{12}) — At t_{11}, S_4 is gated off. C_{r3} and C_{r4} begin to be discharged and charged again. The charge/discharge rate depends mainly on the magnitude of I_{r1} at t_{11}.

Step 13 (t_{12} ~ t_{13}) — At t_{12}, when V_{cr4} attempts to overshoot the positive rail, D_3 is forward biased. The circuit returns to the starting state. Within this period, S_3 can be gated on under zero voltage.

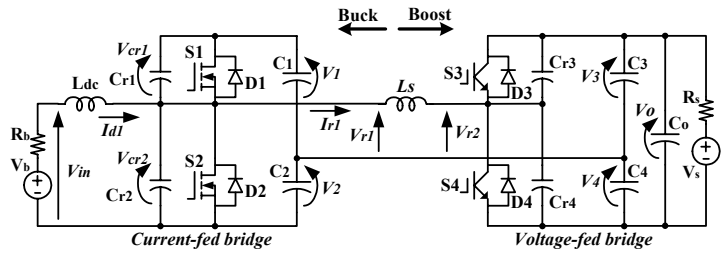

Fig. 3. A primary-referenced equivalent circuit.

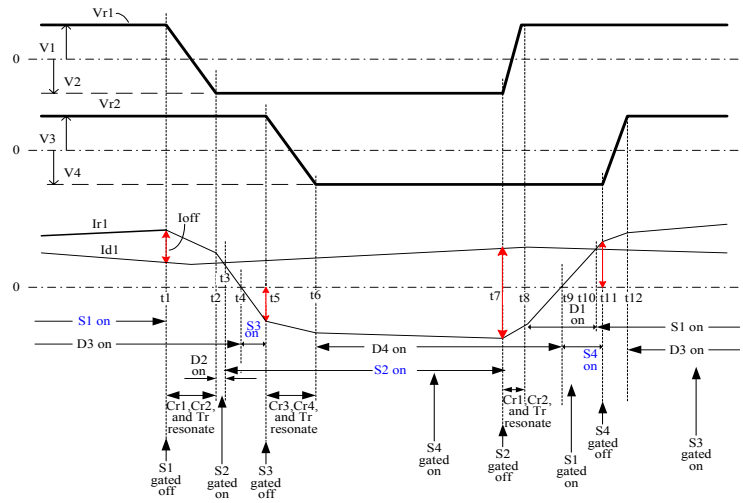
Fig. 4. Waveforms and switching timing in the boost mode.

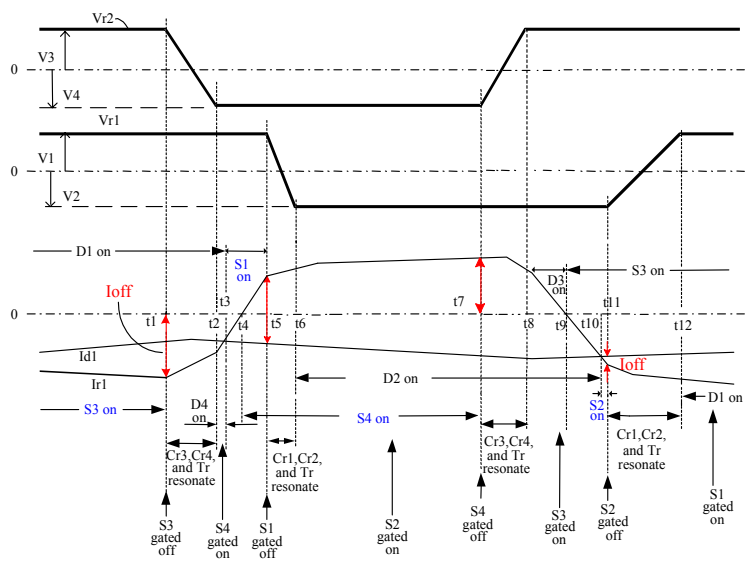
Fig. 5. Waveforms and switching timing in the buck mode.

Because of the topological symmetry of the circuit, the operation principles in the buck mode are similar to those in the boost mode. Fig. 5 describes one switching cycle in the buck mode. Because of the reversed power flow, the phase of the transformer secondary voltage V_{r2} is leading the primary voltage V_{r1}. The starting point of this commutation cycle is selected at the instant when S_3 is going to be turned off. Commutation procedure can be analogously inferred and is omitted.

STEADY STATE ANALYSIS

SOFT COMMUTATION ANALYSIS — The commutation

mechanism in the proposed converter is similar to the diode-to-switch commutation of the auxiliary resonant commutated pole (ARCP) converter [9]; i.e., turn-off of the main conducting device diverts the current to the corresponding snubber capacitors to charge one and discharge the other, resulting in a zero voltage turn-off. The zero voltage turn-on is achieved by gating on the in-coming device while the anti-parallel diode is conducting. However, unlike the ARCP converter, the proposed circuit does not require an auxiliary circuit to achieve soft switching. From Figs. 3 – 5, it is clear that the conditions of soft switching depend on the magnitude of I_{r1} and I_{d1} at t_1, t_5, t_7 and t_{11}. Soft-switching conditions are summarized in Table 1. It should be noted that these equations are for the ideal conditions; i.e. there are no losses in the circuit. In reality, a certain amount of energy must be stored into the transformer leakage inductance before turning off the outgoing switch to ensure ZVS for the incoming switch.

Table 1. Soft-switching conditions.

For the boost mode	For the buck mode
$\begin{cases} I_{r1}(t_1) > I_{d1}(t_1) \\ I_{r1}(t_5) < 0 \\ I_{r1}(t_7) < I_{d1}(t_7) \\ I_{r1}(t_{11}) > 0 \end{cases}$	$\begin{cases} I_{r1}(t_1) < 0 \\ I_{r1}(t_5) > I_{d1}(t_5) \\ I_{r1}(t_7) > 0 \\ I_{r1}(t_{11}) < I_{d1}(t_{11}) \end{cases}$

POWER TRANSFER CHARACTERISTICS — The analysis of static characteristics is based on the primary-referenced equivalent circuit in Fig. 3 and the idealized waveforms in Fig. 6, where ϕ_1 represents the phase shift angle between the transformer primary and secondary voltage waveforms. At steady state, the duty ratio must be fixed at 50%, i.e., $\phi_2=\pi$. There are four operation modes in one switching period, and the relationship between voltage and current in each mode can be established. Assuming $V_1=V_2=V_{in}$, $V_3=V_4=V_o/2$, the transferred power can be found to be:

$$P_o = \frac{V_{in}V_o}{2\omega L_s}\frac{\phi_1(\pi-\phi_1)}{\pi} \tag{1}$$

Where ω is the angular switching frequency, V_{in} the input dc voltage, and V_o the high-side dc bus voltage referred to the primary side.

Equation (1) indicates that, when duty cycle and switching frequency are fixed, the output power is related to phase shift angle and transformer leakage inductance. Fig. 7 plots the output power curves versus the phase shift angle at L_s = 0.6 μH and L_s = 0.3 μH at a switching frequency of 20 kHz. For a given amount of output power, a smaller leakage inductance results in a smaller phase shift angle. To reduce the circulating current and to improve the efficiency, the phase shift angle should be kept as small as possible. Therefore, the leakage inductance needs to be minimized. On the other hand, a higher leakage inductance helps to meet the soft-switching conditions.

DESIGN EQUATIONS — For a given maximum output power, P_{o_max}, at an input dc voltage, V_{in}, a switching frequency, ω, an expected phase shift angle, ϕ_1, the transformer leakage inductance, L_s, can be calculated by

$$L_s = \frac{V_{in}V_o \cdot \phi_1 \cdot (\pi-\phi_1)}{P_{o_\max} \cdot 2\omega\pi}. \tag{2}$$

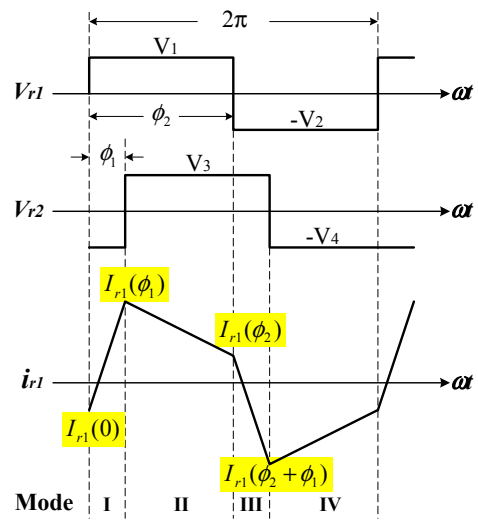

Fig. 6. Idealized voltage and current waveforms of transformer.

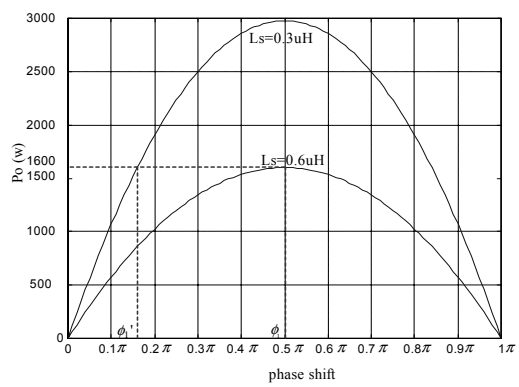

Fig. 7. The output power, ϕ_1, and leakage inductance L_s.

Referring to Fig. 6, the initial states $I_{r1}(0)$, $I_{r1}(\phi_1)$, $I_{r1}(\phi_2)$, $I_{r1}(\phi_1+\phi_2)$ for each of the four modes during one complete switching cycle can be derived based on the boundary conditions:

$$\begin{cases} I_{r1}(0) = -I_{r1}(\phi_2) \\ I_{r1}(\phi_1) = -I_{r1}(\phi_2+\phi_1) \end{cases} \tag{3}$$

At a duty ratio of 50%, i.e. $\phi_2 = \pi$, the boundary points of I_{r1} can be calculated by Eq. (4).

$$\begin{cases} I_{r1}(0) = \dfrac{V_3-V_1}{2\omega L_S}(\pi-\phi_1) - \dfrac{V_1+V_4}{2\omega L_S}\phi_1 \\ I_{r1}(\phi_1) = \dfrac{V_1+V_4}{2\omega L_S}\phi_1 + \dfrac{V_3-V_1}{2\omega L_S}(\pi-\phi_1) \\ I_{r1}(\pi) = -I_{r1}(0) \\ I_{r1}(\pi+\phi_1) = -I_{r1}(\phi_1) \end{cases} \tag{4}$$

Assuming an efficiency of η, the average current of I_{d1} provided by the power supply can be found by

$$I_{d1} = \frac{P_{o_\max}}{\eta V_{in}}. \tag{5}$$

The voltage and current ratings of the LVS devices can be determined based on the operating conditions estimated by

$$\begin{cases} I_{peak} = I_{d1} - I_{r1}(0) \\ V_{peak} = 2V_{in} \end{cases}. \tag{6}$$

The maximum and minimum voltage change rates, *dv/dt*, happen at ωt=0, where the turn-off current is maximum, and ωt=π, where the turn-off current becomes minimum, respectively. Assuming the snubber capacitance is *Cr*, the range of *dv/dt* can be derived as

$$\frac{|I_{r1}(\pi)| - |I_{d1}|}{C_r} \le \frac{dv}{dt} \le \frac{|I_{r1}(0)| + |I_{d1}|}{C_r}. \tag{7}$$

The inductance L_{dc} can be determined for a given peak-to-peak ripple current, ΔI of I_{d1} by

$$L_{dc} = \frac{V_{in}}{2fsw \cdot \Delta I} \tag{8}$$

The soft-switching condition can be verified in the following equation.

$$\text{For boost}\begin{cases} I_{r1}(0) - I_{d1} < 0 \\ I_{r1}(\phi_1) > 0 \\ I_{r1}(\pi) - I_{d1} > 0 \\ I_{r1}(\pi + \phi_1) < 0 \end{cases} \quad \text{for buck}\begin{cases} I_{r1}(0) > 0 \\ I_{d1} > I_{r1}(\phi_1) \\ I_{r1}(\pi) < 0 \\ I_{r1}(\pi + \phi_1) > I_{d1} \end{cases} \tag{9}$$

CHARACTERISTIC CURVES — Characteristic curves are derived based on the design equations. Fig. 8 describes the system behavior in the boost mode when the transformer leakage inductance is 0.6 μH.

Figs.8 (a)–(d) plots the input current, transformer current, *dv/dt(max)*, and *dv/dt*(min) over the full output power range. These curves show that the soft-switching conditions given in Eq. (9) are satisfied over the whole operating range. Fig. 8(e) shows the current stress of the main switches on the LVS and the HVS against output power. The current stress of the HVS switches is calculated based on the primary-referenced circuit. Fig. 8(f) plots the current stress as a function of phase shift ϕ_1 instead of the output power. An interesting feature can be brought to light by examining these figures, which show that the current stresses of the devices are nearly proportional to the phase shift angle. Therefore, if the phase shift is decreased for the same output power, the current stress becomes less. This feature is important to improve the system efficiency because the conduction loss will become dominant in soft-switching converters.

MODELING AND CONTROL SYSTEM DESIGN

Although Pspice-like programs can be used to simulate the detailed performance of switching converters, it is inconvenient and time-consuming to study large-signal long-term dynamic operations. The average model approach is very helpful for control system design and analysis [10–13]. In deriving an average model for the transformer-isolated dc/dc converters using the state-space averaging technique, care should be taken to avoid picking ac variables, such as the current and voltage of the isolation transformer, for the independent variables. A switching-frequency-dependent averaged model was developed for the proposed dc/dc converter and was verified against the detailed circuit simulation.

The developed average model is provided in this section for control system design for the proposed converter. A linearized small-signal model has been derived to predict large- and small-signal characteristics of the converter. The control-to-output transfer function has been generated to provide the information on the poles, zeros, and gain of the open-loop converter. A controller has been designed to stabilize the system around the nominal operating point and to regulate the output voltage against dc input voltage disturbance and/or load variation. The control system was simulated with Matlab/Simulink to verify the system transient performances.

AVERAGE MODEL — The model assumes that the duty cycle equals 50% and the switching processes are instantaneous. The dynamic variables of the converter are chosen to be the phase shift, ϕ_1, inductor current, i_{d1}, and the capacitor voltages, v_1, v_2, v_3, and v_4. The dc averages of all the variables exist. Although the transformer current, i_{r1}, poses a zero dc average over each switching cycle, the average model does yield useful information on the amplitude of the current. The corner points of i_{r1} in Fig. 6 can be approximated as a function of the average values of v_1, v_2, v_3, and v_4. In addition, the average model is dependent of switching frequency because the switching frequency is a possible control variable in the proposed converter. While the details of the model derivation are in [14], the simplified average model can be expressed in Eq. (10).

$$\begin{cases} \dot{\bar{i}}_{d1} = -\frac{R_b}{L_{dc}}\bar{i}_{d1} - \frac{1}{2L_{dc}}\bar{v}_{12} + \frac{1}{L_{dc}}v_b \\ \dot{\bar{v}}_{12} = \frac{1}{C_p}\bar{i}_{d1} - \frac{\phi_1(\pi - \phi_1)}{2\pi \cdot C_p \cdot \omega L_s}\bar{v}_{34} \\ \dot{\bar{v}}_{34} = \frac{\phi_1(\pi - \phi_1)}{2\pi \cdot C_t \cdot \omega L_s}\bar{v}_{12} - \frac{2}{C_t R_s}\bar{v}_{34} + \frac{2}{C_t R_s}v_s \end{cases} \tag{10}$$

where $C_t = C_s + 2C_o$, C_P=C_1=C_2, C_S=C_3=C_4, $\bar{v}_{12} = \bar{v}_1 + \bar{v}_2$, $\bar{v}_{34} = \bar{v}_3 + \bar{v}_4$.

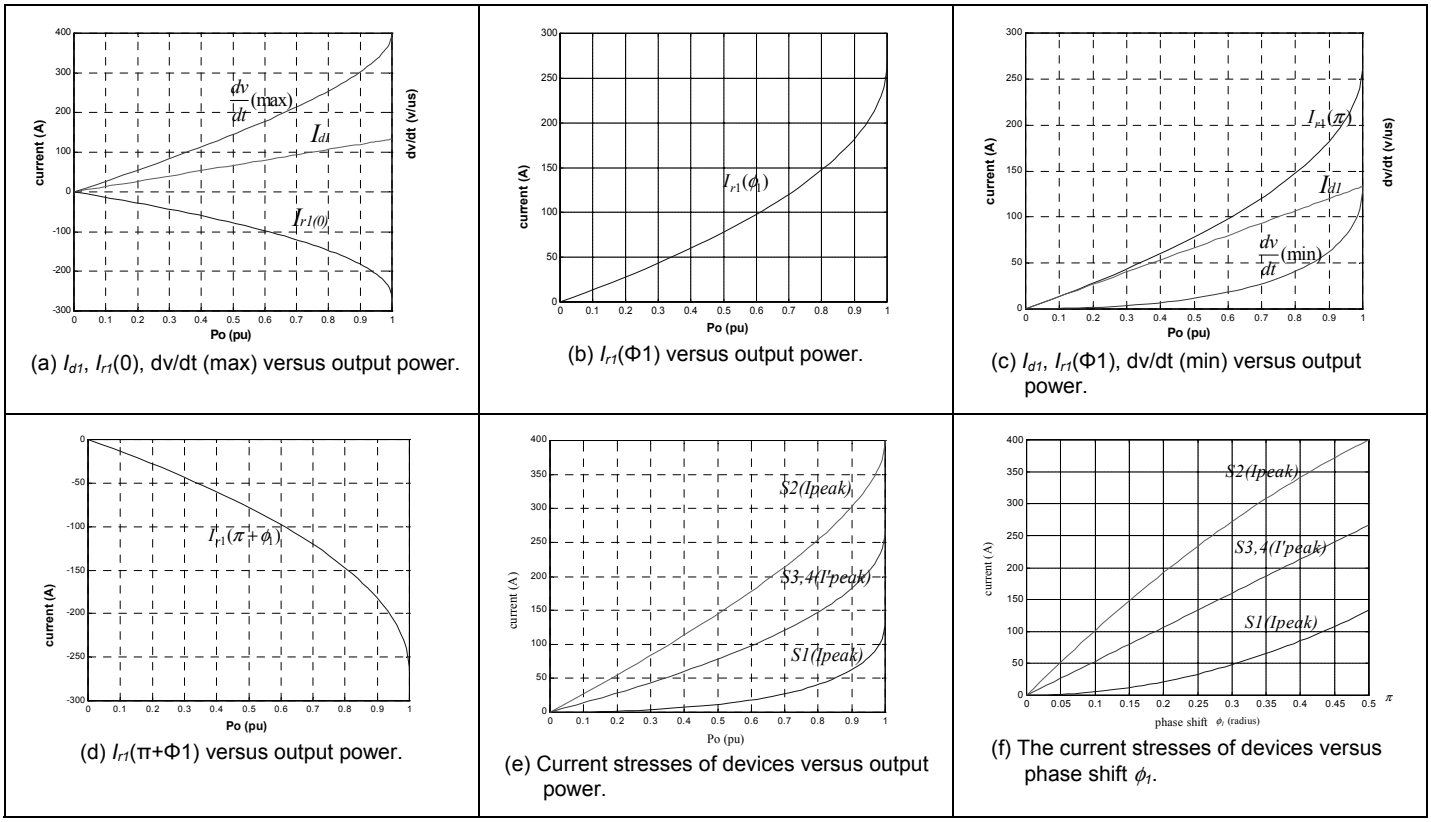

(a) I_{d1}, $I_{r1}(0)$, dv/dt (max) versus output power.

(b) $I_{r1}(\Phi 1)$ versus output power.

(c) I_{d1}, $I_{r1}(\Phi 1)$, dv/dt (min) versus output power.

(d) $I_{r1}(\pi+\Phi 1)$ versus output power.

(e) Current stresses of devices versus output power.

(f) The current stresses of devices versus phase shift ϕ_1.

Fig. 8. Characteristic curves at L_s=0.6μH.

CONTROL SYSTEM DESIGN AND SIMULATION — By introducing small perturbations,

$v_{in} = V_{in} + \tilde{v}_{in}$, $\phi_1 = \Phi_1 + \tilde{\phi}_1$, $i_o = 0 + \tilde{i}_o$, $v_{12} = V_{12} + \tilde{v}_{12}$, $i_{d1} = I_{d1} + \tilde{i}_{d1}$, $v_{34} = V_{34} + \tilde{v}_{34}$, where i_o is a current source placed across the nominal load.

Choosing $(\tilde{i}_{d1},\ \tilde{v}_{12},\ \tilde{v}_{34})$ as state variables, $(\tilde{v}_{in},\ \tilde{\phi}_1,\ \tilde{i}_o)$ as control inputs and $\tilde{v}_{34}$ as controlled output, linearized state equations can be derived as follows:

$$\begin{cases} \begin{bmatrix} \dot{\tilde{i}}_{d1} \\ \dot{\tilde{v}}_{12} \\ \dot{\tilde{v}}_{34} \end{bmatrix} = \begin{bmatrix} 0 & -\dfrac{1}{2L_{dc}} & 0 \\ \dfrac{1}{C_p} & 0 & \dfrac{-2\Phi_1(\pi-\Phi_1)}{K1} \\ 0 & \dfrac{2\Phi_1(\pi-\Phi_1)}{K3} & \dfrac{-2}{C_t R} \end{bmatrix} \begin{bmatrix} \tilde{i}_{d1} \\ \tilde{v}_{12} \\ \tilde{v}_{34} \end{bmatrix} + \begin{bmatrix} \dfrac{1}{Ldc} & 0 & 0 \\ 0 & \dfrac{-2(\pi-2\Phi_1)\cdot V_{34}}{K1} & 0 \\ 0 & \dfrac{2(\pi-2\Phi_1)\cdot 2V_{in}}{K3} & \dfrac{-2}{C_t} \end{bmatrix} \begin{bmatrix} \tilde{v}_{in} \\ \tilde{\phi}_1 \\ \tilde{i}_o \end{bmatrix} \\ \tilde{v}_o = [0 \quad 0 \quad 1]\,[\tilde{i}_1 \quad \tilde{v}_{12} \quad \tilde{v}_{34}]^T \end{cases} \tag{11}$$

where $K1$=4πω$LsCp$, $K3$=4πωLsC_o.

For these nominal operating points:

$P_o = 1.6\ kW$, $V_{in} = 12\ V$, $\Phi_1 = 0.16\pi$, $R_s = 0.36\Omega$, $L_{dc} = 5\ \mu H$, $C_p = C_s = 10\ mF$, $C_o = 169\ mF$, $f_s = 20\ kHz$, and $L_S = 0.3\ \mu H$, the transfer function matrix from input vector to output can be calculated as follows.

$$\begin{aligned} T_1(s) &= \frac{\tilde{v}_o(s)}{\tilde{v}_{in}(s)} = \frac{0.319\times 10^9}{s^3 + 15.964s^2 + 0.100\times 10^8 s + 0.159\times 10^9} \\ T_2(s) &= \frac{\tilde{v}_o(s)}{\tilde{\phi}_1(s)} = \frac{617.048s^2 - 0.343\times 10^6 s + 0.617\times 10^{10}}{s^3 + 15.964s^2 + 0.100\times 10^8 s + 0.159\times 10^9} \\ T_3(s) &= \frac{\tilde{v}_o(s)}{\tilde{i}_o(s)} = \frac{-15.964s^2 - 0.159\times 10^9}{s^3 + 15.964s^2 + 0.100\times 10^8 s + 0.159\times 10^9} \end{aligned} \tag{12}$$

The transfer functions are used to design the controller to allow the converter to meet load regulation and transient response specifications, especially the control-to-output transfer function $T_2(s)$. The root locus plot of $T_2(s)$ is shown in Fig 9. The root locus of the compensated system is shown in Fig. 10, in which a controller is employed as described in Eq. (13).

$$K_c(s) = \frac{K(s + 0.008 + 3160i)(s + 0.008 - 3160i)}{(s + 1000)(s + 2000)} \tag{13}$$

EXPERIMENTAL RESULTS

A 1.6 kW prototype has been built and tested to evaluate its performance. Fig. 11 shows a photo of the prototype. In order to compare with the size of the first-generation converter, the prototype is laid on a 0.375" liquid-cooled heat sink with the same footprint, 7.5" in width by 13.5" in length. The actual occupied area is 7.25" by 8.5", illustrating the high power density characteristic of the second-generation converter. The phase-shift angle was set at 0.04π, namely 1 μs at a 20 kHz switching frequency. The leakage inductance of the transformer in this prototype was measured as 0.4 μH.

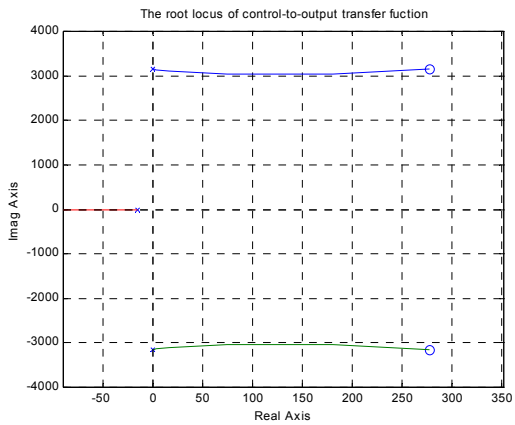

Fig. 9. Root locus plot of $T_2(s)$ of the uncompensated system.

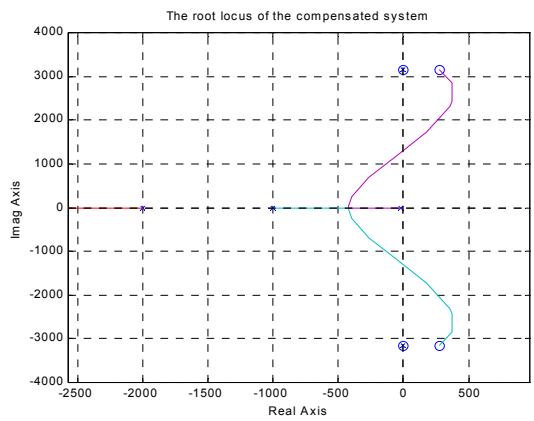

Fig. 10. The root locus of the compensated system.

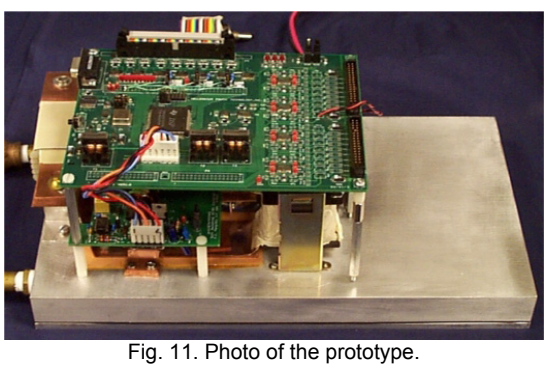

Fig. 11. Photo of the prototype.

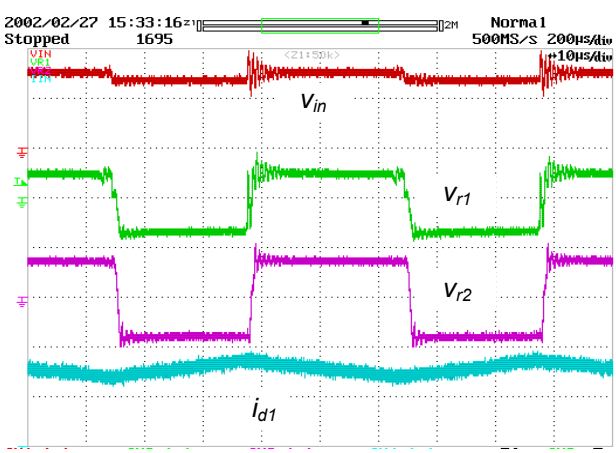

V_{in}: 10 V/div, v_{r1}: 20 V/div, v_{r2}: 200 V/div, i_{d1}: 100 A/div, 10µs/div

Fig.12. Steady state operation in boost mode for P_o=1.77 kW.

Typical testing waveforms in the boost mode are shown in Fig. 12, where the amount of power transferred to the HVS is 1.77 kW, slightly higher than the requirement. The ringing on the rising and falling edges of the transformer primary voltage waveform, v_{r1}, is due to the difficulty of measuring directly the two terminals of the primary side of the transformer because of the tight packaging. Consequently, the measurement loop may be the main reason for this ringing effect.

The details of the switching process of S_2 and S_4 in the buck mode, with a voltage source of 116 V at the HVS and a resistive load of 0.1 Ω at the LVS, are demonstrated in Fig.13. Zero voltage turn-on and turn-off are apparent. Soft switching of the other devices was also observed.

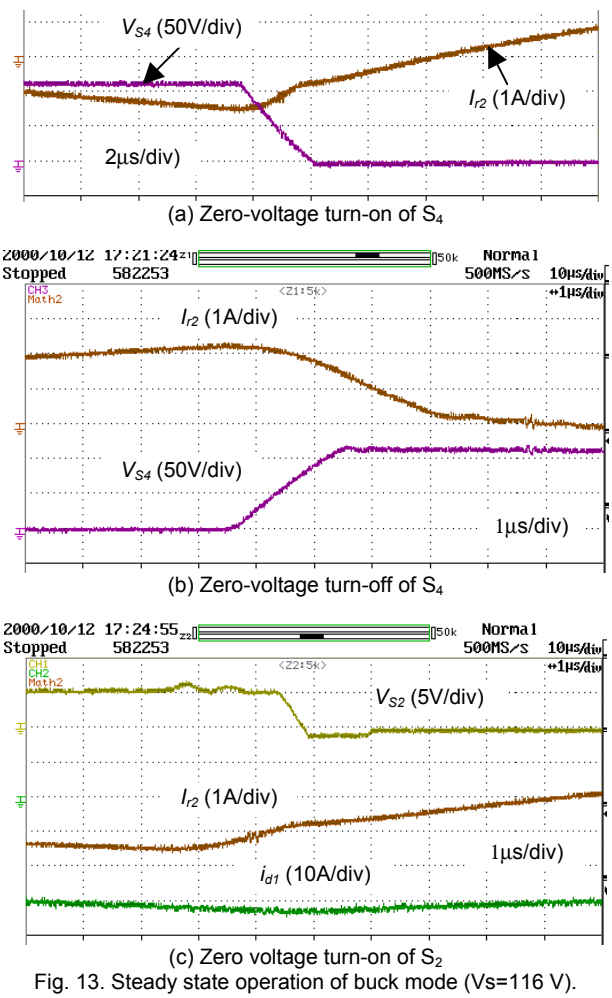

(c) Zero voltage turn-on of S_2

Fig. 13. Steady state operation of buck mode (Vs=116 V).

Fig. 14 presents the output voltage characteristics of the converter from zero to full power under open-loop control. As indicated in the figure, the trace marked by * is the experimental result, the one marked by “o” is the result of the detailed circuit simulation, and the third one marked with “+” is the result of the average model simulation. The close agreement among the three curves confirms the validity of the average model. The differences among the average model, detailed circuit model, and testing results on the prototype can be explained as follows. The average model assumes ideal switches and components; there are no losses in the

switches, capacitors, inductor and transformer. The detailed circuit model is a better approximation of the actual circuit because some of the losses mentioned have been taken into account. However, accurately modeling the device losses and magnetic losses in the prototype is impossible in the detailed circuit simulation. Therefore, the output voltage of the average model is higher than that of the detailed circuit model, and the detailed circuit model voltage is higher than the testing results on the prototype.

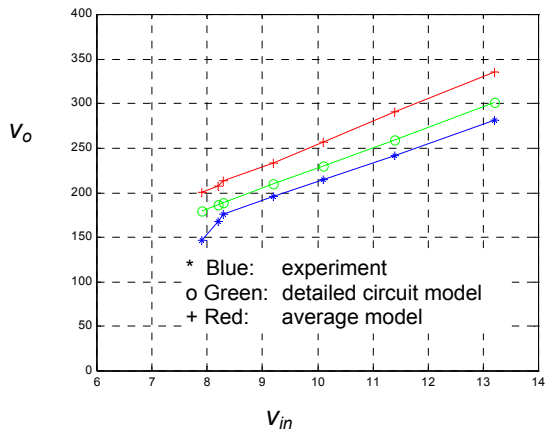

Fig. 14. Comparison of low-to-high output voltage characteristics under open loop control.

CONCLUSION

This paper presents a soft-switched bi-directional dc/dc converter for FCPEV applications. Compared with the first-generation and other soft-switched bi-directional dc/dc converters, this topology has the following features:

- Fewer switching devices.
  Compared with the full-bridge topologies, this converter has half the number of switching devices. This reduction also leads to significant savings on the gate drive and accessory power requirements.
- No auxiliary circuit or complex control dedicated for soft switching.

Extensive simulation based on a detailed circuit and an average model verified the circuit operation and soft-switching conditions. The average model further produced design equations. A prototype rated at 1.6 kW was designed, built, and successfully tested in the laboratory. This topology, therefore, provides a solution for low-cost, lightweight, compact, and reliable dc/dc converter designs for automotive applications. Other application areas are in uninterrupted power supplies and battery charging and discharging systems.

REFERENCES

1. T. Gilchrist, "Fuel cells to the fore," *IEEE Spectrum*, November 1998.
2. R. L. Steigerwald, "High-frequency resonant transistor dc/dc converters," *IEEE Trans. Ind. Electron.*, Vol. IE-3, no. 2, pp.181–191, May 1984.
3. M. Jain, M. Daniele and P. K. Jain, "A bidirectional dc-dc converter topology for low power application," *IEEE Trans. Power Electronics*, vol.15, No.4, pp. 595–606, July 2000.
4. T. Reimann, S. Szeponik, G. Berger, and J. Petzoldt, "A novel control principle of bi-directional dc/dc power conversion," in *Conf. Rec. 1997 IEEE Power Electronics Specialist Conf.*, pp. 978–984.
5. D. M. Divan and O. Patterson, "A pseudo resonant full bridge dc/dc converter," in *Conf. Rec. 1987 IEEE Power Electronics Specialist Conf.*, pp.424–430.
6. R. Watson et al., "A soft-switched, full-bridge boost converter employing an active-clamp circuit," in *Conf. Rec. 1996 IEEE Power Electronics Specialist Conf.*, pp.1948–1954.
7. R. W. DeDonker, D. M. Divan, and Kheraluwala, "Power conversion apparatus for dc/dc conversion using dual active bridges," U. S. Patent, no. 5,027,264
8. M. H. K. Wang et al, "Bi-directional dc to dc converters for fuel cell systems," in *Conf. Rec. 1998 IEEE Power Electronics In Transportation*, pp. 47–51.
9. R. W. DeDonker and J. P. Lyons, "The auxiliary resonant commutated pole converter," *IEEE IAS Annu. Meet. Conf. Rec.*, pp. 1228–1235, 1990.
10. R. D. Middlebrook and S. Cuk, "A general unified approach to modeling switching-converter power stages," *IEEE Power Electronics Conf.*, pp. 18–34, 1976.
11. P. T. Krein, J. Bentsman, R. M. Bass, and B. C. Lesieutre, "On the use of averaging for analysis of power electronic systems," *IEEE Trans. Power Electronics*, vol. 5, No. 2, pp. 182–190, April 1990.
12. B. Lehman and R. M. Bass, "Switching frequency dependent averaged models for PWM DC-DC converters," *IEEE Trans. Power Electronics*, vol.11, No.1, pp.89–98, January 1996.
13. B. Lehman and R. M. Bass, "Extension of averaging theory for power electronic systems," *IEEE Trans. Power Electronics*, vol. 11, No. 4, pp. 542–553, July 1996.
14. H. Li, Fang Z. Peng, and J. Lawler, "Modeling, simulation, and experimental verification of soft-switched bi-directional DC-DC converters," *IEEE APEC proceeding*, 2001, pp.736–742.

CONTACT

Gui-Jia Su, Ph.D., Senior R&D Staff

Oak Ridge National Laboratory
National Transportation Research Center
2360 Cherahala Blvd.
Knoxville, TN 37932
Phone: (865) 946-1330, Fax: (865) 946-1262
Email: sugj@ornl.gov